Table of Contents

Table S1. The antibodies and ELISA kits used in this research.

Target	Vendor	Catalog No.	Clone
CD9 (biotin)	Ancell	156-030/mono mouse	C3-3A2
CD63 (biotin)	Biolegend	353018/mono mouse	H5C6
CD81 (biotin)	Ancell	302-030/mono mouse	1.3.3.22
CD81	Ancell	302-820/mono mouse	1.3.3.22
EpCAM (biotin)	Abcam	ab187270/mono mouse	MOC-31
EpCAM	Biolegend	324202/mono mouse	9C4
EpCAM ELISA kit	R&D Systems	DY960	
CD24 (biotin)	eBioscience	13-0247-80/mono mouse	SN3 A5-2H10
CD24	R&D Systems	AF5247	poly
FRα (biotin)	R&D Systems	BAF5646/poly goat	poly
FRα ELISA kit	R&D Systems	DY5646	
CA125 (biotin)	GeneTex	GTX44293/mono mouse	X306
CA125	Abcam	ab1107/mono mouse	X75
HER-2 (biotin)	eBioscience	BMS120BT/mono mouse	2G11
HER-2	eBioscience	BMS120/mono mouse	2G11
EGFR (biotin)	Abcam	ab24293/mono mouse	EGFR1
EGFR	BD Bioscience	555996/mono mouse	EGFR1
IgG (FITC)	Life Technologies	34-152-110413/ poly goat	poly

Table S2. Plasma samples used in Figure 5.

Samples for Exosome Profiling					
OvCa patients	**Age**	**Stage**	**Histology**	**Pathology**	**Tissue**
1	72	IIIC	High grade serous adenocarcinoma	Malignant	
2	67	IIA	High grade papillary serous carcinoma	Malignant	
3	70	IIIC	High grade serous carcinoma	Malignant	
4	80	IIIC	Metastatic high grade papillary serous carcinoma	Malignant	
5	66	IV	Metastatic high grade serous carcinoma	Malignant	
6	65	IIIB	High grade serous carcinoma	Malignant	
7	66	IIIC	High grade serous carcinoma	Malignant	
8	64	IIIC	High-grade serous adenocarcinoma	Malignant	Tested
9	61	IIIC	Metastatic high grade papillary serous carcinoma	Malignant	
10	53	IIIC	High grade papillary serous adenocarcinoma	Malignant	
11	74	IIA	High grade serous carcinoma	Malignant	Tested
12	55	IIIA	Metastatic ovarian carcinoma	Malignant	
13	75	IIIC	Mixed epithelial carcinoma: serous and endometrioid (50%)	Malignant	Tested
14	53	IIIC	High grade serous carcinoma	Malignant	
15	65	IIA	Mucinous adenocarcinoma	Malignant	
16	65	IIIC	High grade serous carcinoma	Malignant	
17	58	IA	Mucinous cystadenocarcinoma	Malignant	
18	58	IIIC	High grade serous carcinoma	Malignant	
19	51	IIA	Low grade serous carcinoma	Malignant	
20	63	IIA	Serous adenocarcinoma	Malignant	
Non-cancer control	**Age**	**Stage**	**Histology**	**Pathology**	**Tissue**
21	51	n/a	No history of cancer	Control	
22	53	n/a	No history of cancer	Control	
23	50	n/a	No history of cancer	Control	
24	52	n/a	No history of cancer	Control	
25	53	n/a	No history of cancer	Control	
26	52	n/a	No history of cancer	Control	
27	54	n/a	No history of cancer	Control	
28	56	n/a	Benign inclusion cysts	Benign	
29	67	n/a	Mucinous cystadenoma	Benign	
30	58	n/a	Serous cystadenoma	Benign	
Samples for Western Blot					
OvCa patients	**Age**	**Stage**	**Histology**	**Pathology**	**Tissue**
1	73	n/a	Benign inclusion cysts	Benign	
2	50	IA	Mucinous cystadenocarcinoma	Malignant	
3	65	IIIC	High grade serous carcinoma	Malignant	
4	79	IV	Metastatic high grade serous carcinoma	Malignant	

Table S3: Sample size calculation with desired errors.

		Type I error- α	
		0.05	0.20
Type II error- β	0.05	12 + 24	6.5 + 13
	0.20	7.5 + 15	3 + 6

Table S4. Results of one-way ANOVA and post hoc Tukey's test of the difference among the control, early-stage (stage I/II), and advanced (stage III/IV) groups.

Exosome Marker	Overall ANOVA	Homogeneity of Variance (Levene's test)	Tukey's Test between Groups		
			Control/Early	Early/Advanced	Control/Advanced
CD24	SD p = 3.6E-12	NS p = 0.24	SD p = 5.6E-9	NS p = 0.06	SD p = 2.4E-11
EpCAM	SD p = 6.2E-10	NS p = 0.18	SD p = 2.2E-6	NS p = 0.23	SD p = 5.0E-10
FRα	SD p = 6.1E-12	SD p = 0.01	SD p = 2.1E-6	SD p = 0.002	SD p = 2.7E-11

SD: significantly different; NS: not significant. Significance level was set at $p < 0.05$.

Supplementary Figures

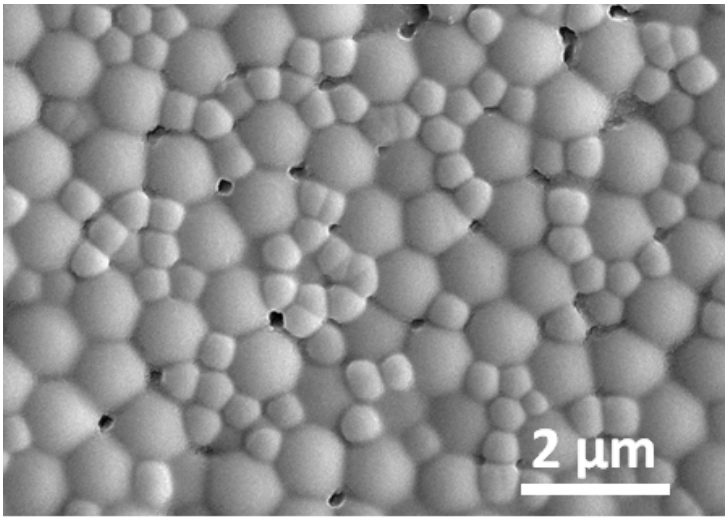

Figure S1. Fabrication of a solid-HB chip. A 520/960 nm binary colloidal structure was assembled and then treated by 10% 3-MPS to fill the interior pores, resulting in a solid-HB micropattern with the nano-textured surface.

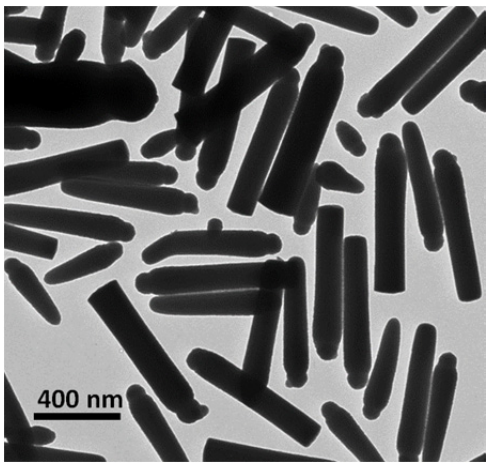

Figure S2. TEM image of synthesized monodisperse silica nanorods. The average diameter and length were determined to be 238 ± 32 nm and 1.34 ± 0.26 μm, respectively.

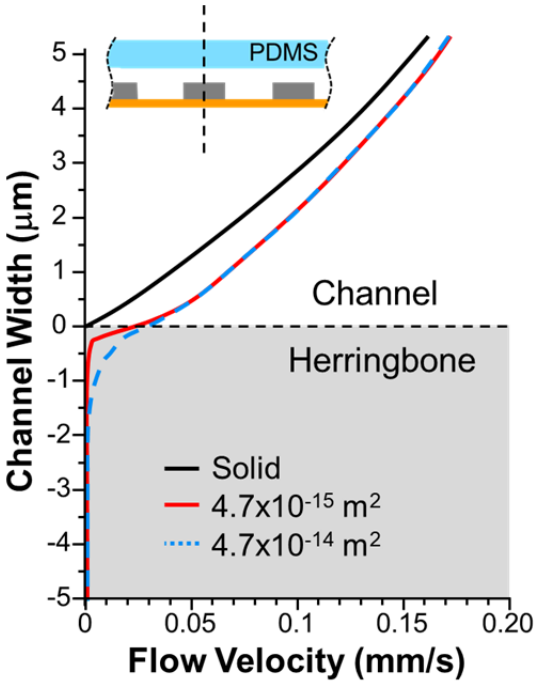

Figure S3. Simulated velocity profiles near the liquid-solid interface. The vertical velocity profile across the center of a HB element was examined, as indicated by the dashed line. The non-slip flow near the boundary between the HB structure and the free-flow domain is modified due to flow penetration into the nanoporous HBs. Such modification of the boundary flow and the flow rate inside the nanoporous domain increase as the permeability increases from 4.7×10^{-15} to 4.7×10^{-14} m^2.

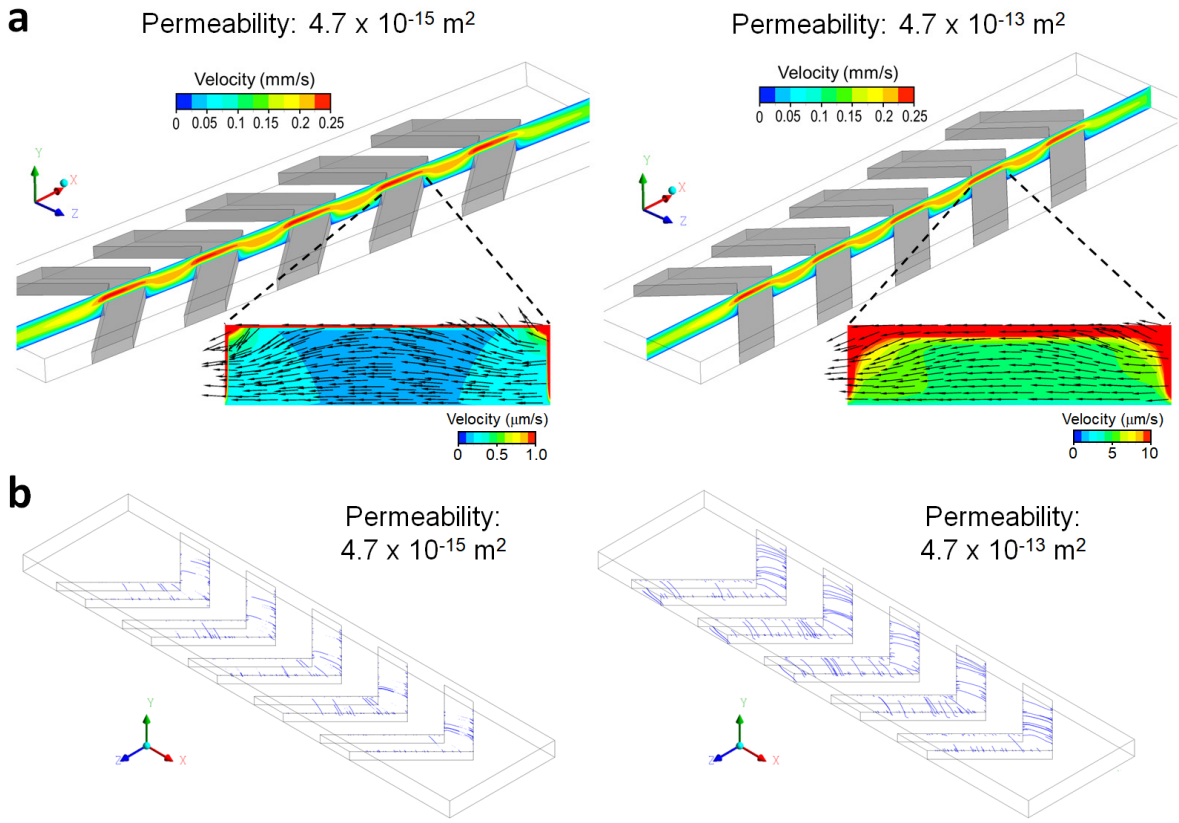

Figure S4. Effects of permeability on particle interactions with the nanodomain. (**a**) Simulation results showing the streamwise flow profiles along the channel length at two values of permeability. The insets highlight the flow patterns inside the nanoporous domains. Color contours indicate the velocity magnitude, while vectors represent the flow direction. (**b**) The plots of particle paths that enter the nano-HBs with variable permeability. Particles were evenly distributed on the inlet and injected at the same time. For clarity, only the trajectories within the nanostructures for the particles that have entered the nano-HBs along their path over a unit of five elements were displayed. At the low permeability (4.7 $\times 10^{-15}$ m^2), ~7.6% of the particles enter the nano-HBs and almost all of the interaction occurs at the corners of the structure where the flow can actually penetrate into the nanostructures. More particles can penetrate into the nanostructures with the higher permeability (4.7 $\times 10^{-13}$ m^2). The flow rate was 0.5 μL/min in all cases.

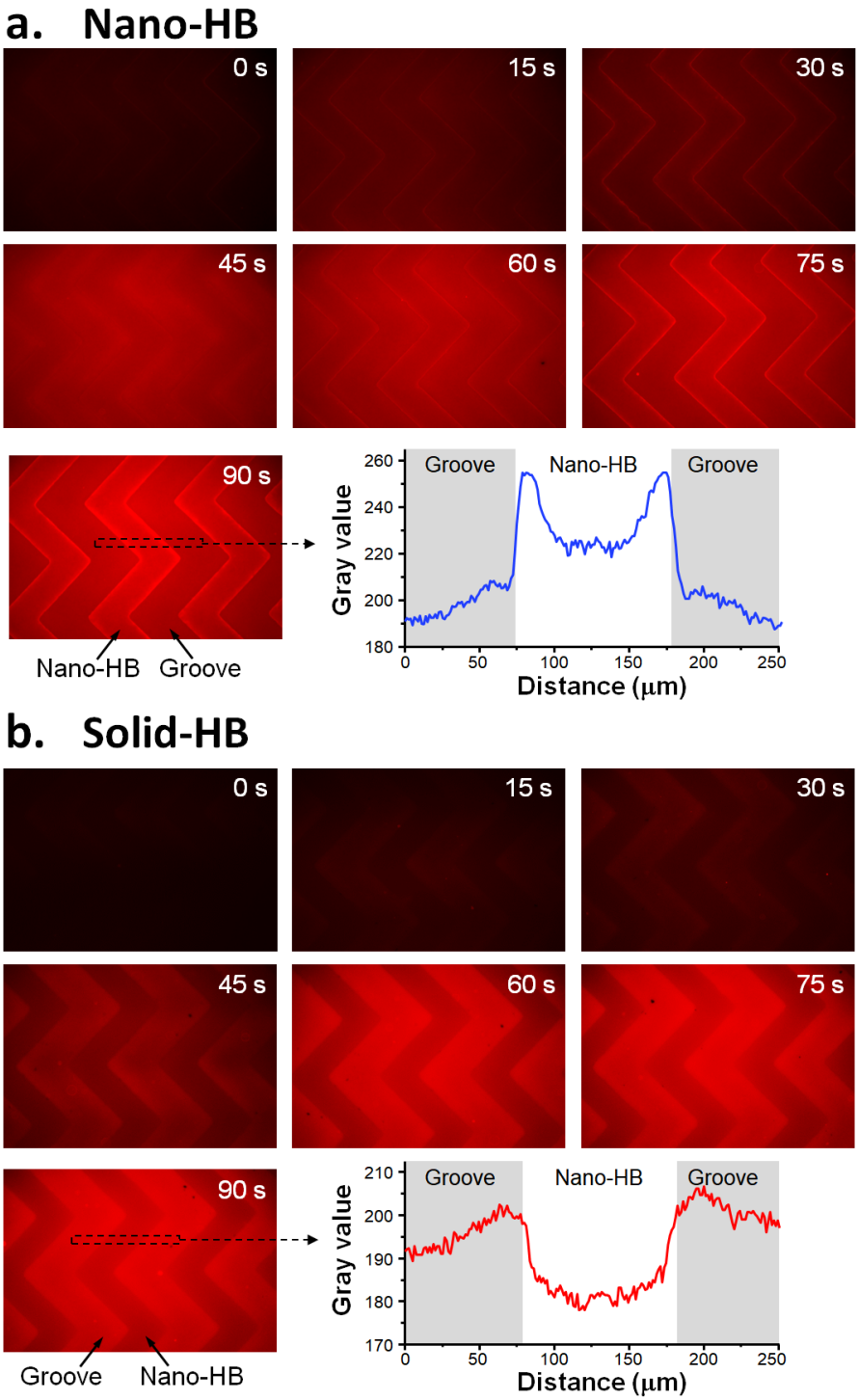

Figure S5. Representative time-lapse epifluorescence microscopy images for the flow experiments in Fig. 2e and 2f. 1:100 diluted solution of FluoSpheres™ microspheres (actual size: 0.046 μm, Ex 540 nm/Em 560 nm) was injected into the channel at 0.5 μL/min by a syringe pump. Intensity profile across a nano- or solid-HB structure was measured by scanning laterally the area indicated by the black dashed rectangle, respectively. (**a**) The images and the intensity plot show high intensity inside the nano-HB than that the grooves, indicating NPs flowing into the pores. Moreover, the intensity plot suggests that NPs were concentrated on the edges of nano-HBs. (**b**) No flow penetration and NP enrichment were observed with the solid-HBs.

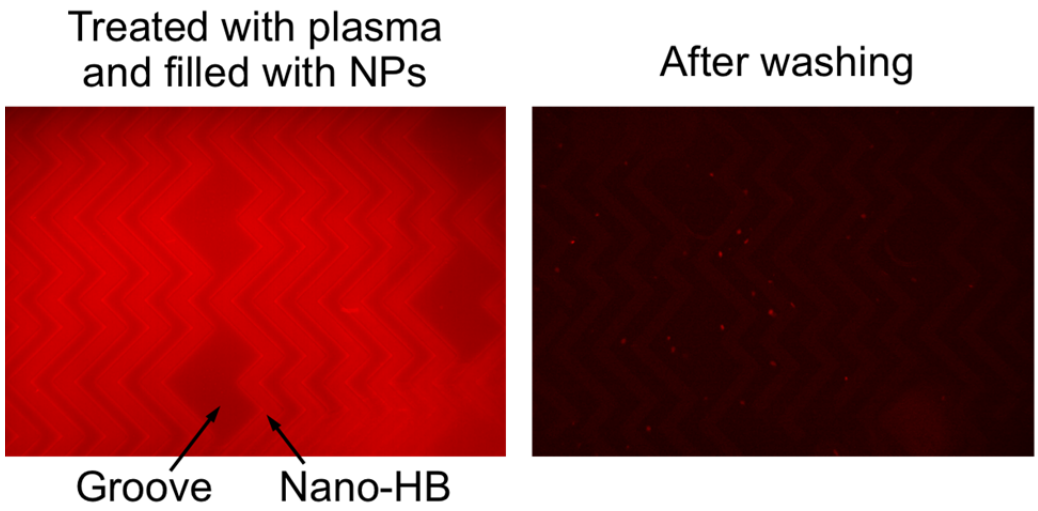

Figure S6. Nanoparticle filling and removal in a nano-HB chip. A nano-HB chip was first flushed with 2 μL human plasma and then filled with 46-nm fluorescent NPs as described in Figure S5. The plasma pretreatment did not appear to noticeably block the nanoporous structure and thus reduce the amount of 46-nm NPs entering the nano-HBs. When washing the chip with PBS at 1 μL/min, NPs in the nano-HBs were mostly washed away within 5 min, faster than the diffusion-driven washing.

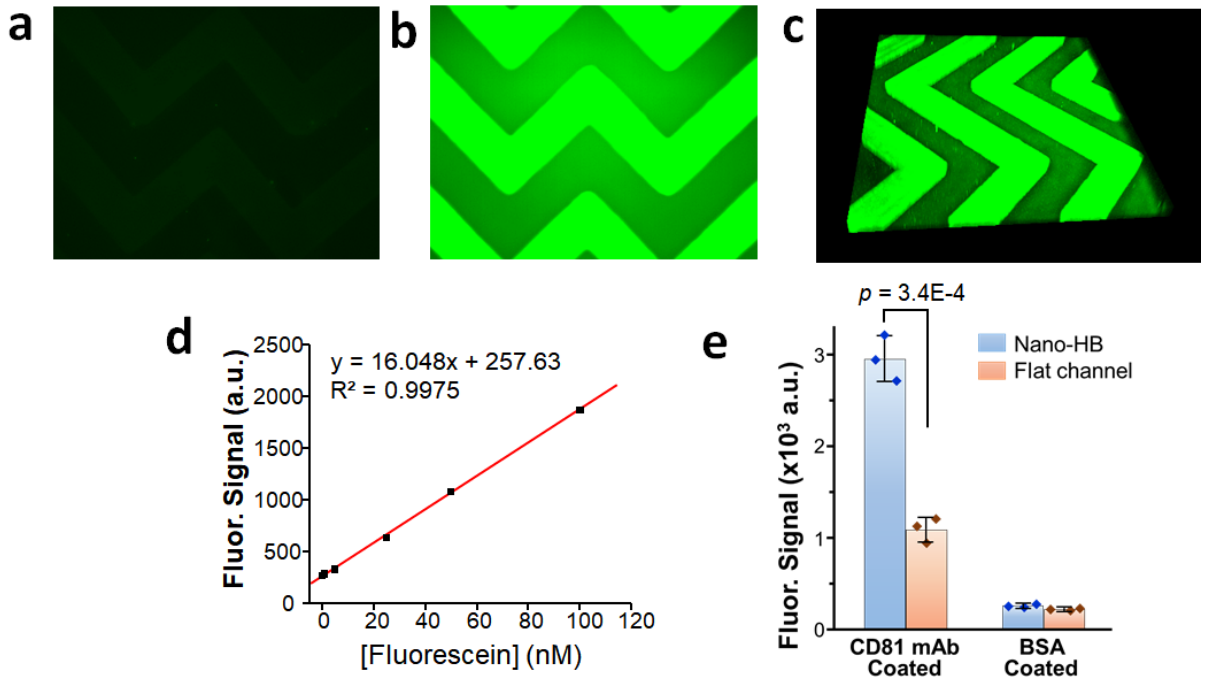

Figure S7. 3D nano-HBs greatly enhance surface antibody immobilization. (**a, b**) Representative fluorescence images of the nano-HB chips after coating with either BSA (**a**) or CD81 antibody (**b**), followed by detection with FITC-labeled anti-IgG secondary antibody. (**c**) 3D confocal fluorescence microscopy imaging verifies that the internal surface of nano-HBs was coated with CD81 mAb. (**d**) Calibration plot of a series dilution of fluorescein in water. (**e**) Comparison between a nano-HB chip and a flat-channel chip showing significant improvement in antibody immobilization by the nano-HB structure (p = 3.4E-4). Low background signal was detected on the BSA-coated chips, which verifies specific detection of the surface-immobilized antibody. For each case, three chips were coated and imaged at five locations to determine the mean fluorescence intensity and S.D. Surface density of antibody was calculated from the measured fluorescence intensity using the calibration curve in (**d**) and assuming an absorbed monolayer of 10 nm thick (IgG dimensions: ~14.5 × 8.5 × 4.0 nm)[1]. The antibody quantity per unit area of the channel surface was determined to be 51.6 ± 8.4 fmol/mm^2 for the flat channels and 167.7 ± 15.5 fmol/mm^2 for the nano-HB chips (mean ± S.D.). Hypothesis testing was done by the two-tailed Student's t-test with the significance level at $p < 0.05$.

1. Bagci, H., Kohen, F., Kuscuoglu, U., Bayer, E.A., Wilchek, M. Monoclonal Anti-Biotin Antibodies Simulate Avidin in the Recognition of Biotin. *Febs Letters* **322**, 47–50 (1993).

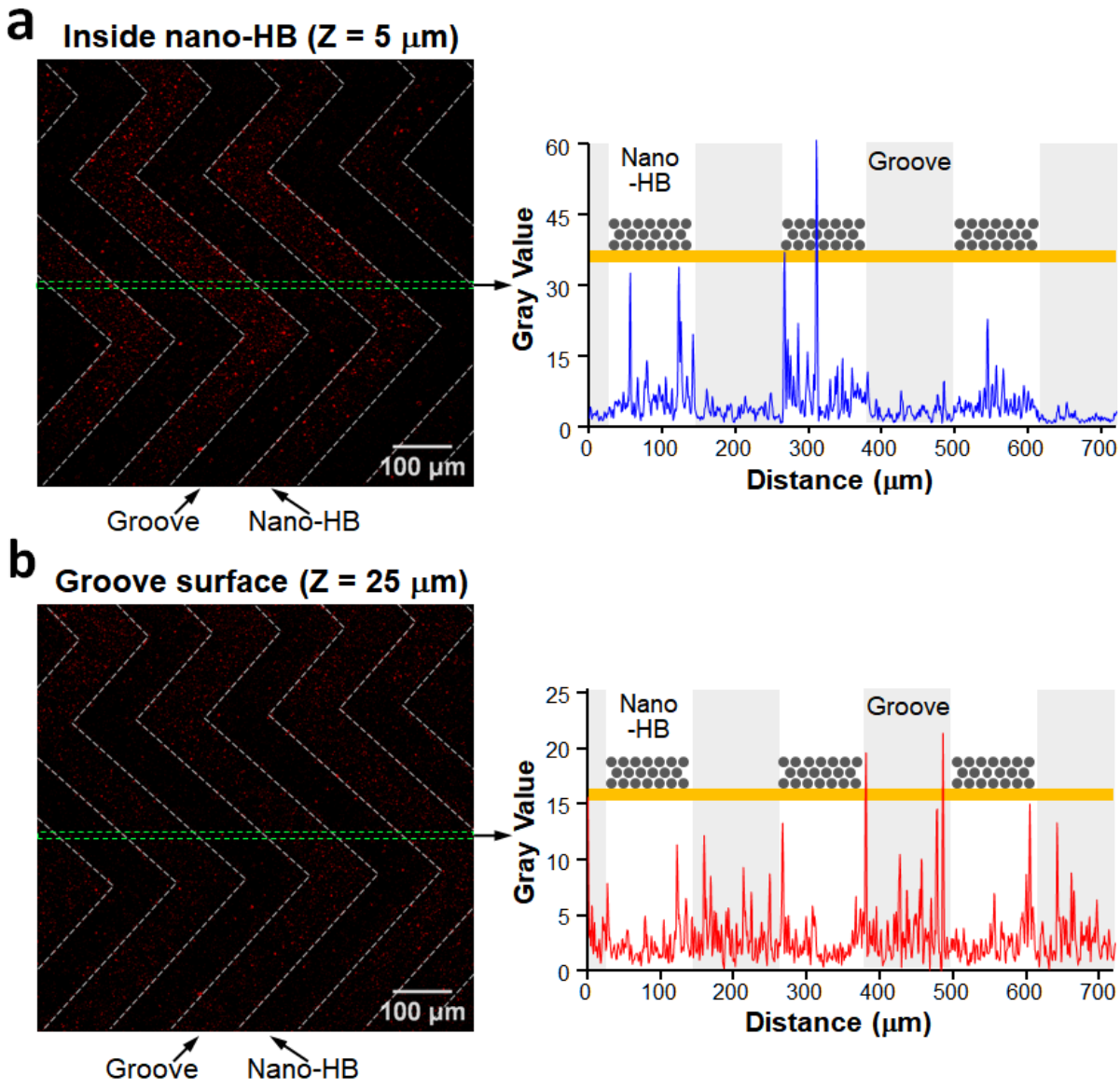

Figure S8. Two slices from the stack of 2D confocal fluorescence microscopy images used to construct the 3D image in Figure 3d. These images (left) were acquired at a Z-location either (**a**) ~5 μm below the top surface of nano-HB structure (Z = 5 μm) and (**b**) on the groove surface (Z = 25 μm). White dashed lines were added to indicate the boundaries between the nano-HB structures and grooves. Corresponding intensity profiles (right) were measured by scanning laterally across the two fluorescence images at the same location, as indicated by the green dashed rectangles. Both fluorescence image and the intensity profile in (**a**) show that many COLO-1 exosomes were captured on the edges of and inside the nano-HB structures. In contrast, when imaged at the level of groove surface (**b**), the number of exosomes captured inside the nano-HBs decreases significantly, while more exosomes were captured on the groove surface as well as the edges of the nano-HBs.

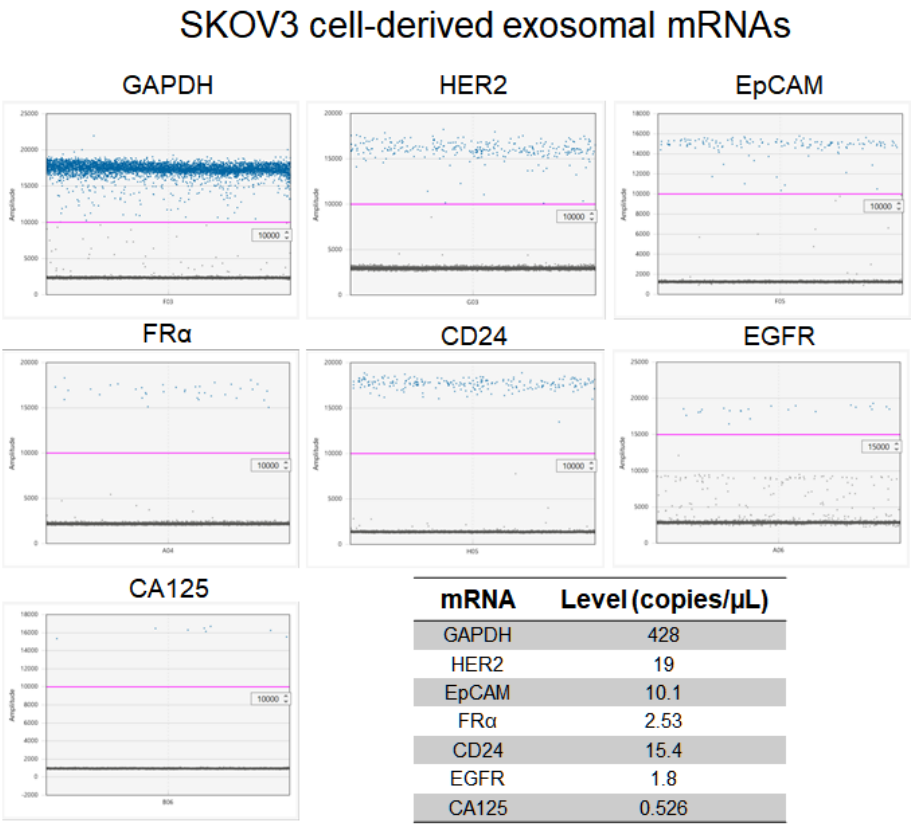

mRNA	Level (copies/μL)
GAPDH	428
HER2	19
EpCAM	10.1
FRα	2.53
CD24	15.4
EGFR	1.8
CA125	0.526

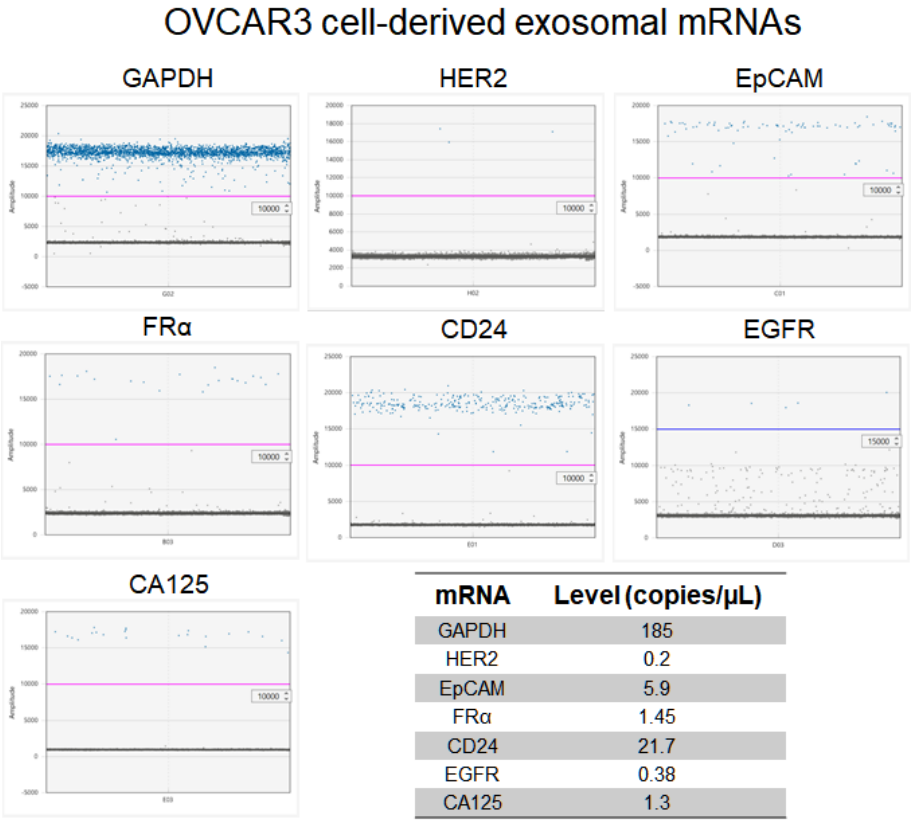

mRNA	Level (copies/μL)
GAPDH	185
HER2	0.2
EpCAM	5.9
FRα	1.45
CD24	21.7
EGFR	0.38
CA125	1.3

Figure S9. Representative results from droplet digital PCR (ddPCR) experiments for mRNA profiling of EVs isolated from two OvCa cell lines by UC.

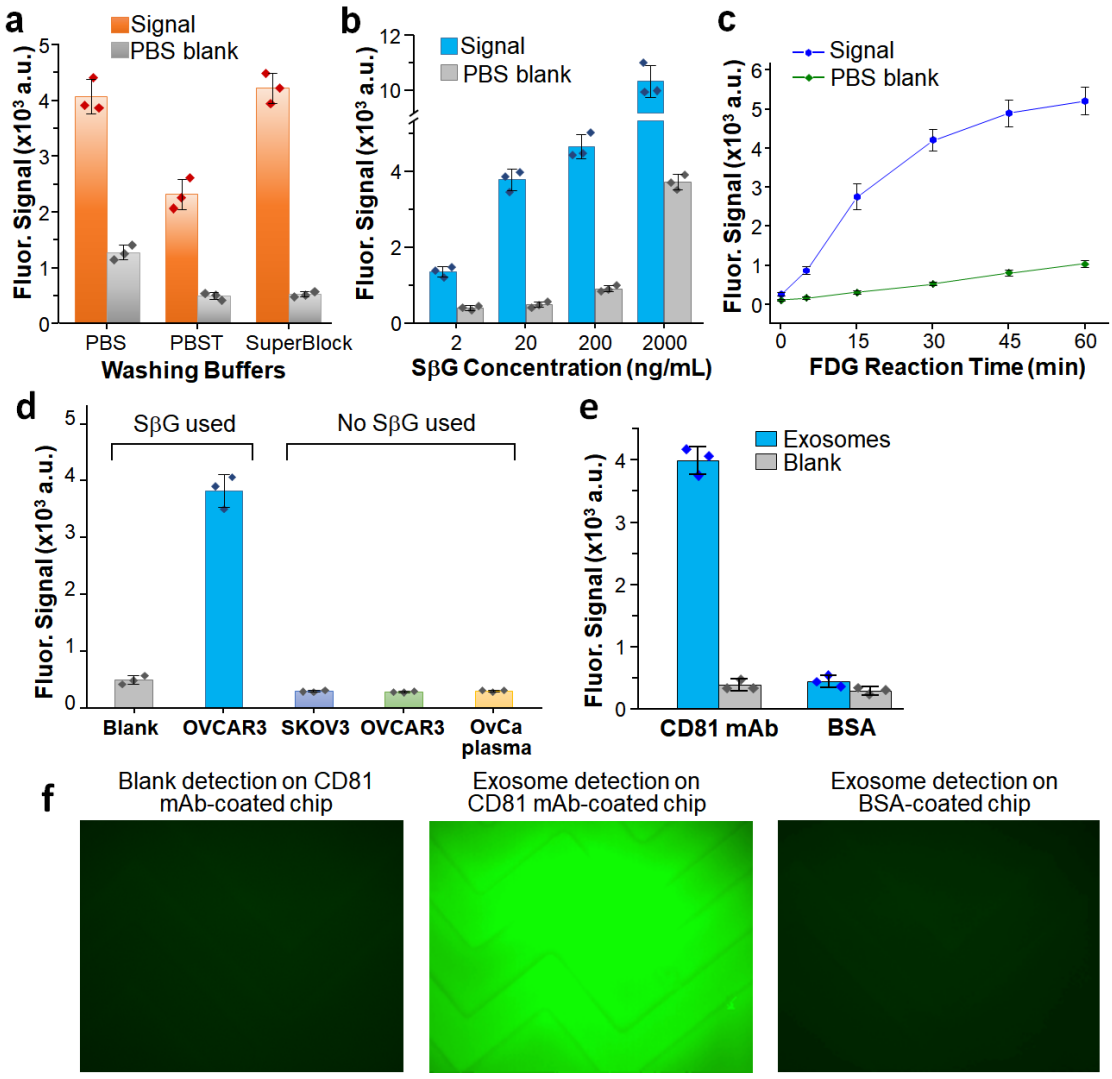

Figure S10. **Optimization of exosome immuno-detection on 3D nano-HB chips.** (**a-c**) Optimization of washing buffer (**a**), reporter enzyme concentration (**b**), and reaction time (**c**) for enzymatic signal amplification to improve the signal-to-noise ratio (SNR) of the sandwich ELISA detection of COLO-1 exosomes. As seen in (**a**), compared to PBS and PBST (PBS with 1% BSA and 0.05% Tween 20), the commercial SuperBlock buffer results in the best SNR. Optimal SβG concentration and FDG incubation time were determined to be 20 ng/mL (**b**) and 30 min (**c**), respectively. The assay conditions were detailed in the Methods section of Supporting Informtion. (**d**) Testing the potential effects of endogenous β-galactosidase in exosomes on the fluororescence detection using β-galactosidase-based signal amplification. UC-purified EVs from three cell lines and OvCa patient plasma (10^6 μL^{-1}) were assayed on chip to form the immunocomplexes and then incubated with the FDG substrate without labeling the immunocomplexes with SβG. For comparison, a PBS blank and an OVCAR3 exosome sample (10^5 μL^{-1}) were assayed by the complete procedure including SβG labeling, as performed above. Very low fluorescence signals were observed for exosome detection without using SβG, while the measurements with SβG led to a slightly higher background level for the blank, due to the non-specific adsorption of SβG, and a very strong signal for exosome detection. These results indicate that endogenous β-galactosidase in exosomes should have no interference with the exosome immunoassay. (**e**) Bar graph and (**f**) representative fluorescence images of detecting PBS blank and COLO-1 exosomes using nano-HB chips coated with anti-CD81 mAb or BSA only. Error bars, one

S.D. (n = 3).

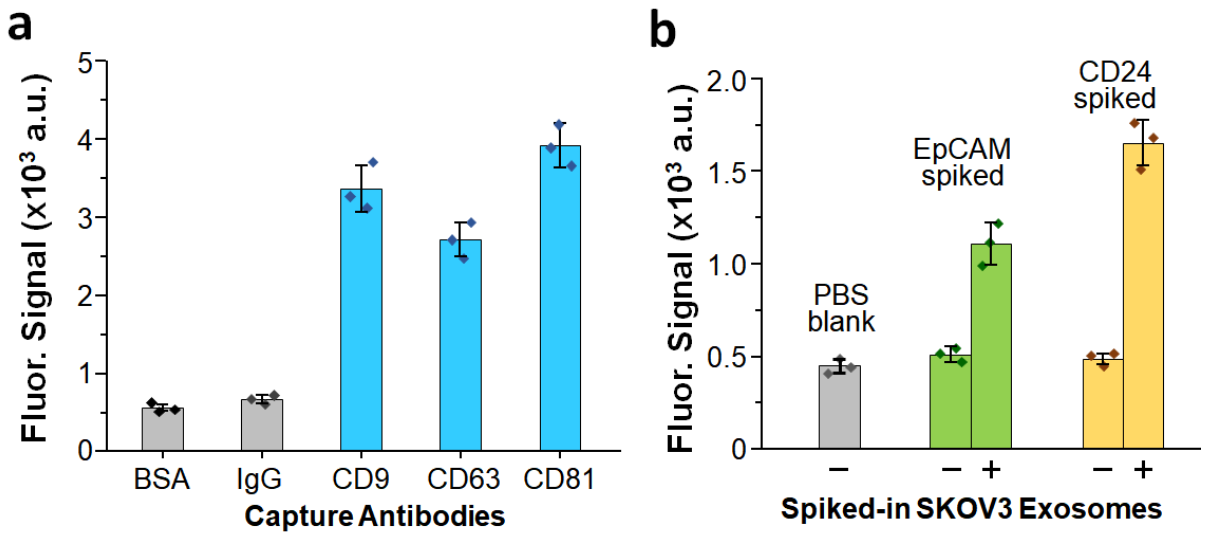

Figure S11. Evaluation of antibodies for capture and detection of OvCa exosomes. (**a**) Optimization of capture antibodies. UC-purified OVCAR3 EVs (10^5 μL^{-1}) were measured on nano-HB chips coated with BSA, normal human IgG and different capture mAbs to assess their efficiency and specificity. A mixture of biotinylated CD9, CD63 and CD81 mAbs was used to detect the captured exosomes. (**b**) Evaluation of the specificity of antibodies for detection of exosomes against free proteins. EpCAM or CD24 protein (10 ng/mL) was spiked in PBS. At the absence of SKOV3 EVs, on-chip analysis of EpCAM-spiked solution using anti-CD81 capture mAb and anti-EpCAM detection mAb reported a signal level very close to that for measuring the PBS blank with a mix of EpCAM and CD24 mAbs. The same assay at the presence of SKOV3 EVs (10^5 μL^{-1}) resulted in a significant increase in detection signal ($p < 0.01$). The same observation was obtained for analysis of CD24 spiked samples using anti-CD24 mAb ($p < 0.0001$). These results verified that the CD81 capture Ab has no significant cross-reactivity with the spiked proteins and the detection Abs, which permits specific immuno-detection of targeted exosomes against free protein contaminants in plasma. Error bars indicate one S.D. (n = 3).

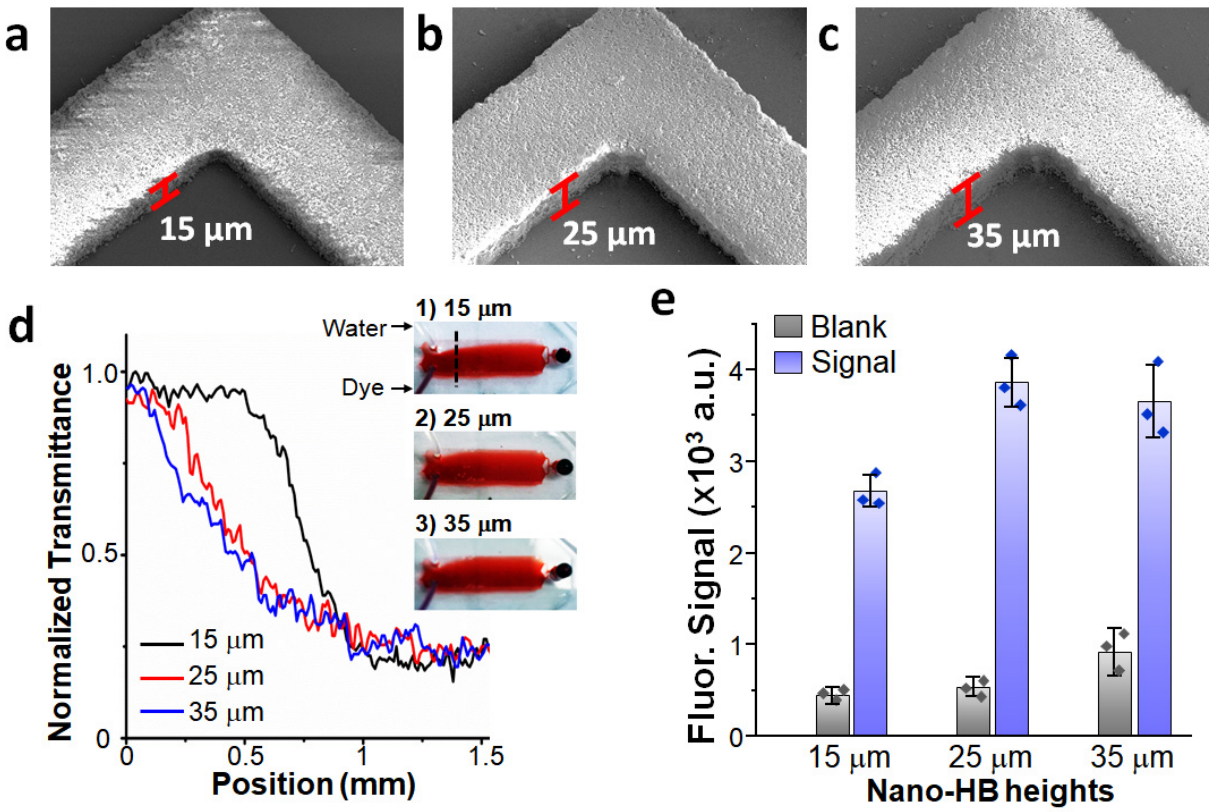

Figure S12. Optimization of the height of nano-HB for exosome detection. (**a-c**) SEM images of the nano-HBs with 15, 25 and 35 µm height, respectively. (**d**) Comparison of the flow mixing efficiency of the nano-HBs of variable heights. Nano-HBs were embedded within a 50-µm tall assay channel; water and dye solution were pumped through the channel in parallel at the same flow rate (1 µL/min). As shown by microscopic imaging (inset) and profiling the cross-sectional concentration gradient, the 25 and 30-µm tall nano-HBs provide better mixing efficiency than the 15-µm structure. (**e**) Comparative studies of nano-herringbones of variable heights for exosome detection. 10^5 μL^{-1} COLO-1 EVs were run through the chips for exosome capture by anti-CD81 mAb and detection by a mixture of mAbs against CD9, CD63 and EpCAM. The 25-µm tall nano-HB afforded the best signal/noise ratio for exosome detection. In all cases, the nano-HBs were fabricated using 960-nm silica particles. Error bars indicate one S.D. (n = 3).

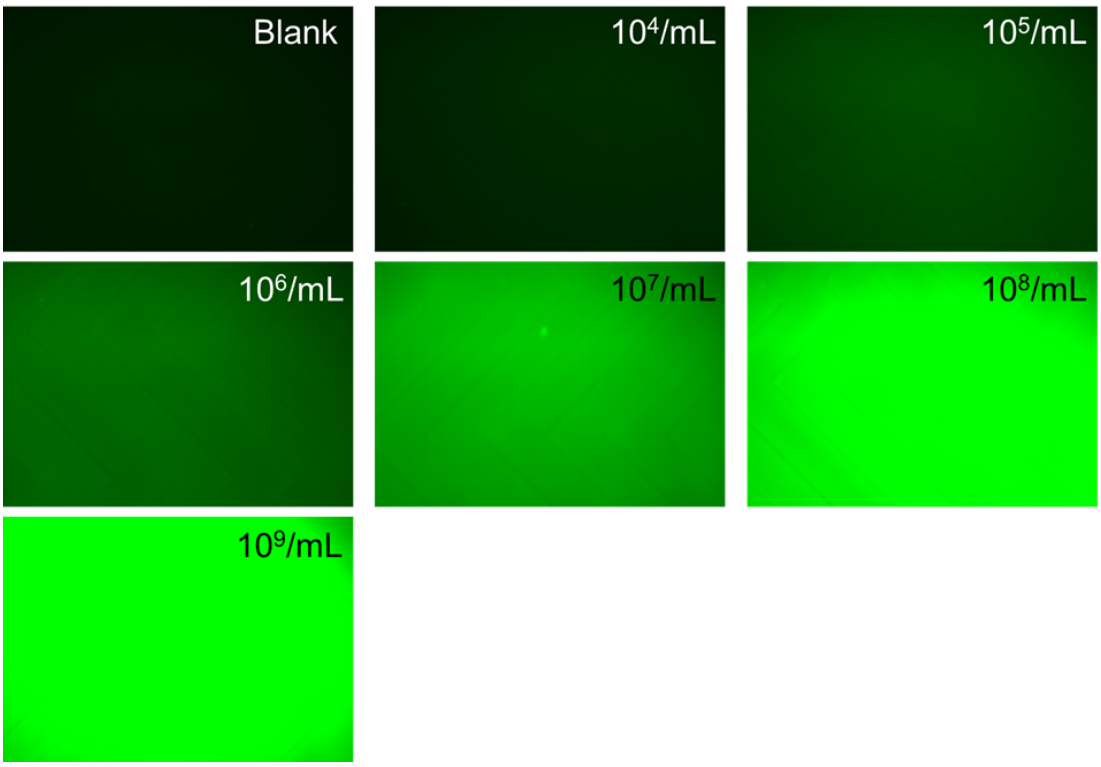

Figure S13. Representative fluorescence images for quantitative detection of COLO-1 exosomes presented in Figure 4b.

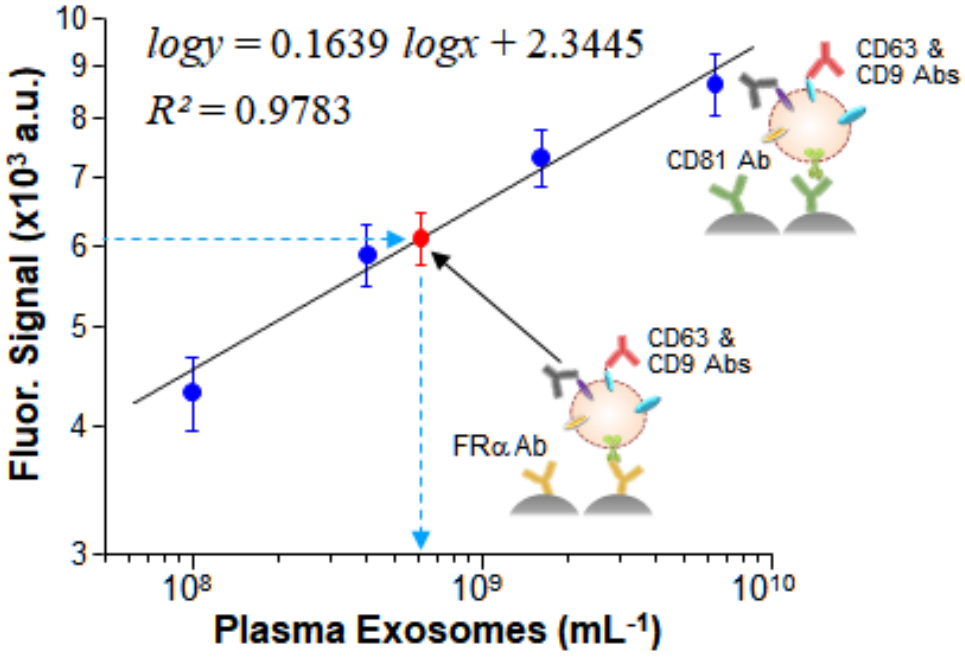

Figure S14. Quantification of relative abundance of FRα+ exosomes in clinical plasma. The plasma from Patient #8 was found to have an EV concentration of 6.4×10^{10} mL^{-1} measured by ultracentrifugation isolation and NTA counting. A series of dilutions were prepared by diluting the plasma with PBS. The calibration plot was obtained by detecting total exosomes with anti-CD81 mAb for exosome capture and a mix of anti-CD9 and CD63 mAbs for detection. A diluted plasma of 6.4×10^9 mL^{-1} was assayed to quantify the FRα+ exosomes using anti-FRα mAb for exosome capture and a mix of anti-CD9 and CD63 mAbs for detection. The data point is shown in red on the plot. We assume that CD9 and CD63 are evenly expressed on every vesicle. Other assay conditions were the same as in Figures 4f and 5a. Error bars indicate one S.D. (n = 3). Using the calibration plot, the concentration of FRα+ exosomes in the 6.4×10^9 mL^{-1} sample was determined to be $2.9 \pm 0.5 \times 10^8$ mL^{-1}. The fraction of FRα+ exosomes was calculated to be 4.5 ± 0.8%.

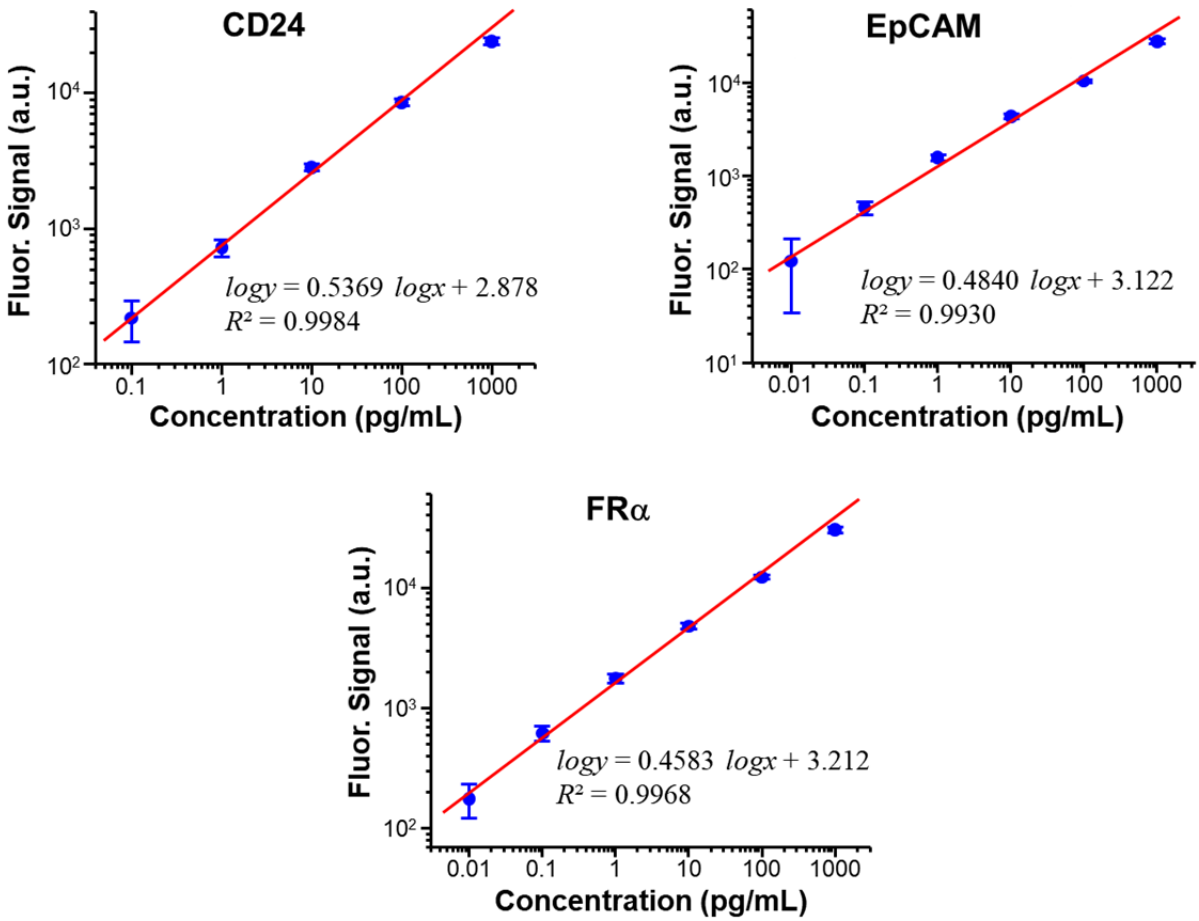

Figure S15. Calibration curves for quantifying three proteins by nano-HB chips. The measured signals were subtracted by the background levels and plotted as a function of protein concentration. The background signals measured from PBS blank using the antibody pairs for individual proteins were: 674 ± 56 a.u. for CD24, 596 ± 51 a.u. for EpCAM, and 572 ± 38 a.u. for FRα. The flow conditions were the same as in the measurements of exosomes in clinical plasma samples in Figure 5a. All measurements were run in triplicate and the background-corrected results are displayed as mean ± S.D. Calibration plots were obtained by fitting with linear least-squares regression and used to convert the fluorescence readout measured for individual exosomal markers in clinical plasma samples to protein concentration.

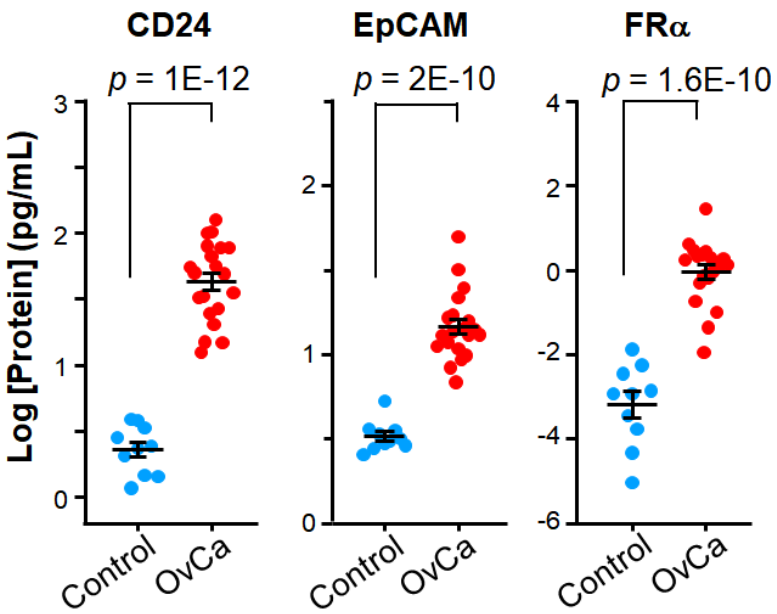

Figure S16. Scatter dot plots of the exosomal expression levels of three biomarkers in the control and OvCa patients. Hypothesis testing was performed with the two-tailed Student's *t*-test. Error bars indicate the mean and one standard error of the mean (s.e.m.). The significance level was set at $p < 0.05$ for all the statistical analyses.

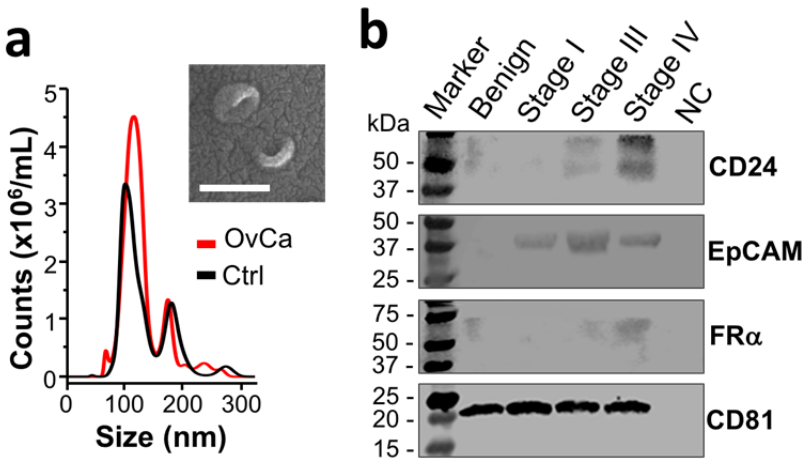

Figure S17. Characterization of EVs isolated from plasma by UC. (**a**) Representative size profiles of vesicles isolated from benign and patient plasma samples by ultracentrifugation and measured by NTA. Inset, typical SEM image of vesicles purified from patient plasma. Scale bar, 100 nm. (**b**) Western blot of CD24, EpCAM, and FRα expression in exosomes from a benign control and OvCa patients of various stages with CD81 as the loading control and 10 μg BSA as negative control (NC).

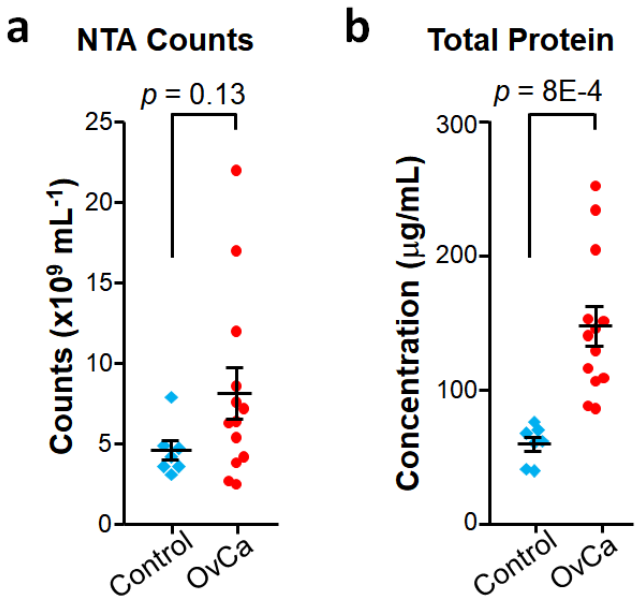

Figure S18. Scatter dot plots for (a) the NTA counting and (b) the Bradford assay of total protein levels of EVs purified from control and patient plasma samples by UC. Hypothesis testing was performed with the two-tailed Student's *t*-test. The error bars in the dot plots indicate the mean and one s.e.m.

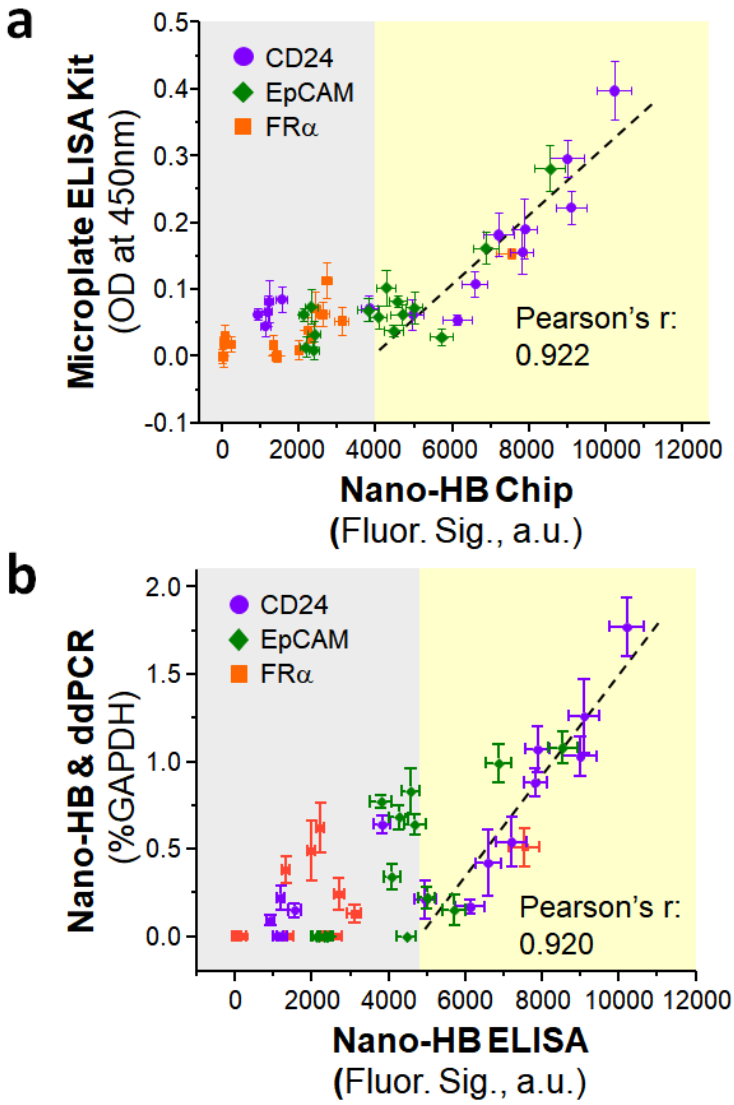

Figure S19. Correlation between the nano-HB chip and two standard methods for plasma sample analysis. (**a**) The data sets from the microplate and nano-HB ELISA measurements displayed reasonably good overall correlation (Pearson's r = 0.831). For the data points in high-concentration range, for example, >4000 a.u. fluorescence intensity (yellow area), statistical analysis by the two-tailed Student's t test showed a Pearson coefficient of 0.922. The microplate ELISA showed decreased sensitivity at low concentrations. (**b**) The correlation between the combined nano-HB capture and ddPCR assay and the nano-HB ELISA (Pearson's r = 0.806). Statistical analysis of the data points with >4700 a.u. fluorescence intensity (yellow area) showed a Pearson coefficient of 0.920. The set of 15 samples were assayed for three exosomal biomarkers, CD24, EpCAM and FRα, as shown in Figure 5b. The optical density and fluorescence signals were subtracted by the background measured with PBS. All measurements were conducted in triplicate and the mean values with one S.D. were plotted.

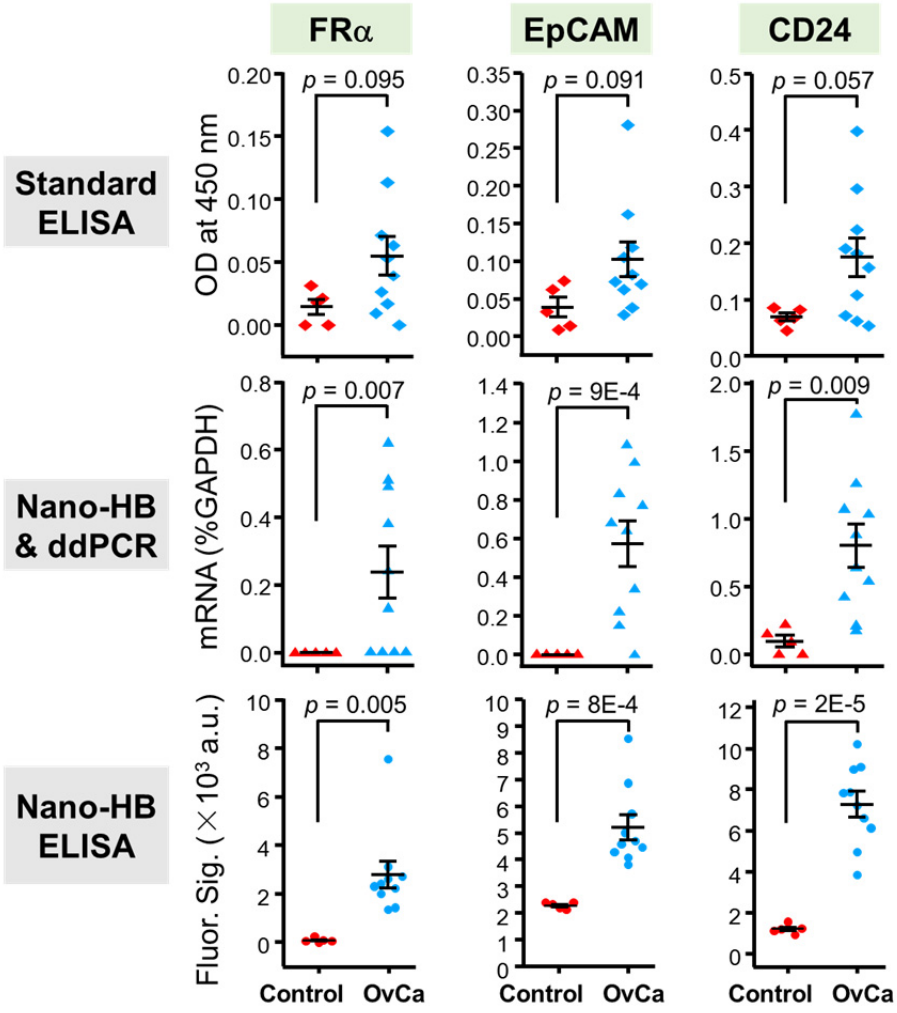

Figure S20. Comparison of diagnostic performance of exosome analysis using the nano-HB ELISA chip and two standard methods. Three exosomal markers in the OvCa (n = 10) and control groups (n = 5) were assayed by the nano-HB ELISA, the microplate ELISA, and the combined nano-HB capture and ddPCR of mRNAs. OvCa patient and control IDs are the same as in Figure 5 and Table S2. Optical density was measured at 450 nm (OD_{450}). The two-tailed Student's t-test was used for statistical comparison at a significance level of $p < 0.05$. All measurements were run in triplicate and the mean values were displayed with one s.e.m.

Patient #4

mRNA	Level (copies/μL)
GAPDH	82.1
CD24	1.02
EpCAM	0.696
FRα	0.523

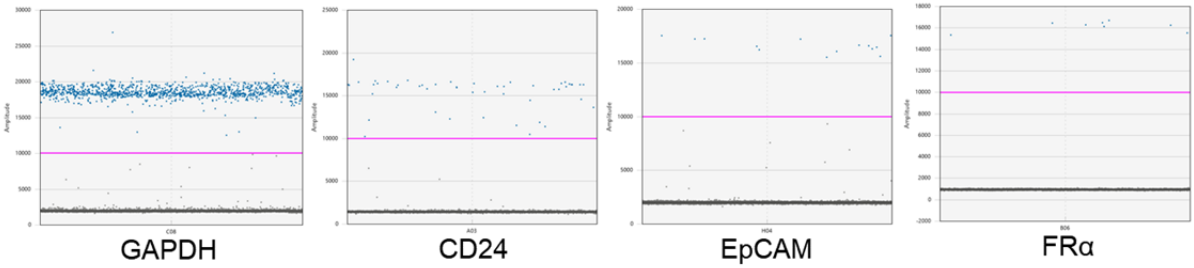

Patient #8

mRNA	Level (copies/μL)
GAPDH	87.9
CD24	1.53
EpCAM	1.08
FRα	0.379

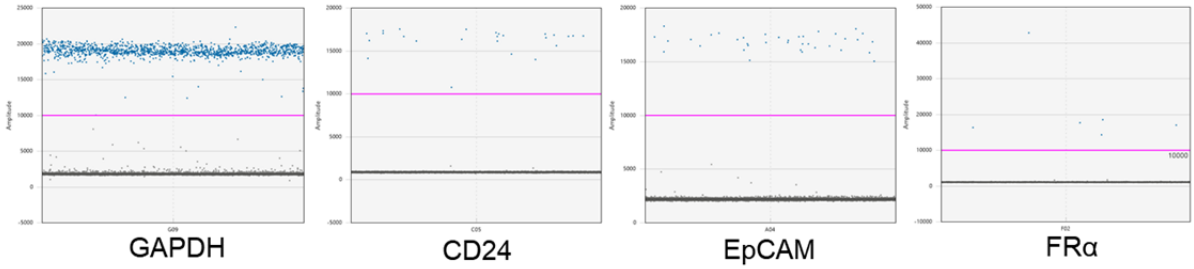

Control #21

mRNA	Level (copies/μL)
GAPDH	55.9
CD24	0.124
EpCAM	0
FRα	0

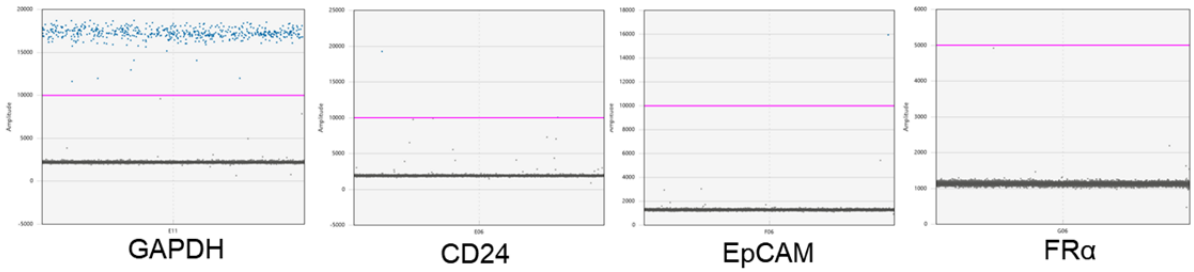

Figure S21. Representative results for nano-HB chip based ddPCR analysis of exosome mRNA markers in clinical plasma samples. 100 μL plasma samples were diluted by 10 times and run through two 8-channel nano-HB chips in parallel to capture exosomes in 2 h. Anti-CD81 mAb was used for exosome capture. Captured exosomes were eluted out and total RNA was extracted for ddPCR detection of individual targets following the standard protocols.

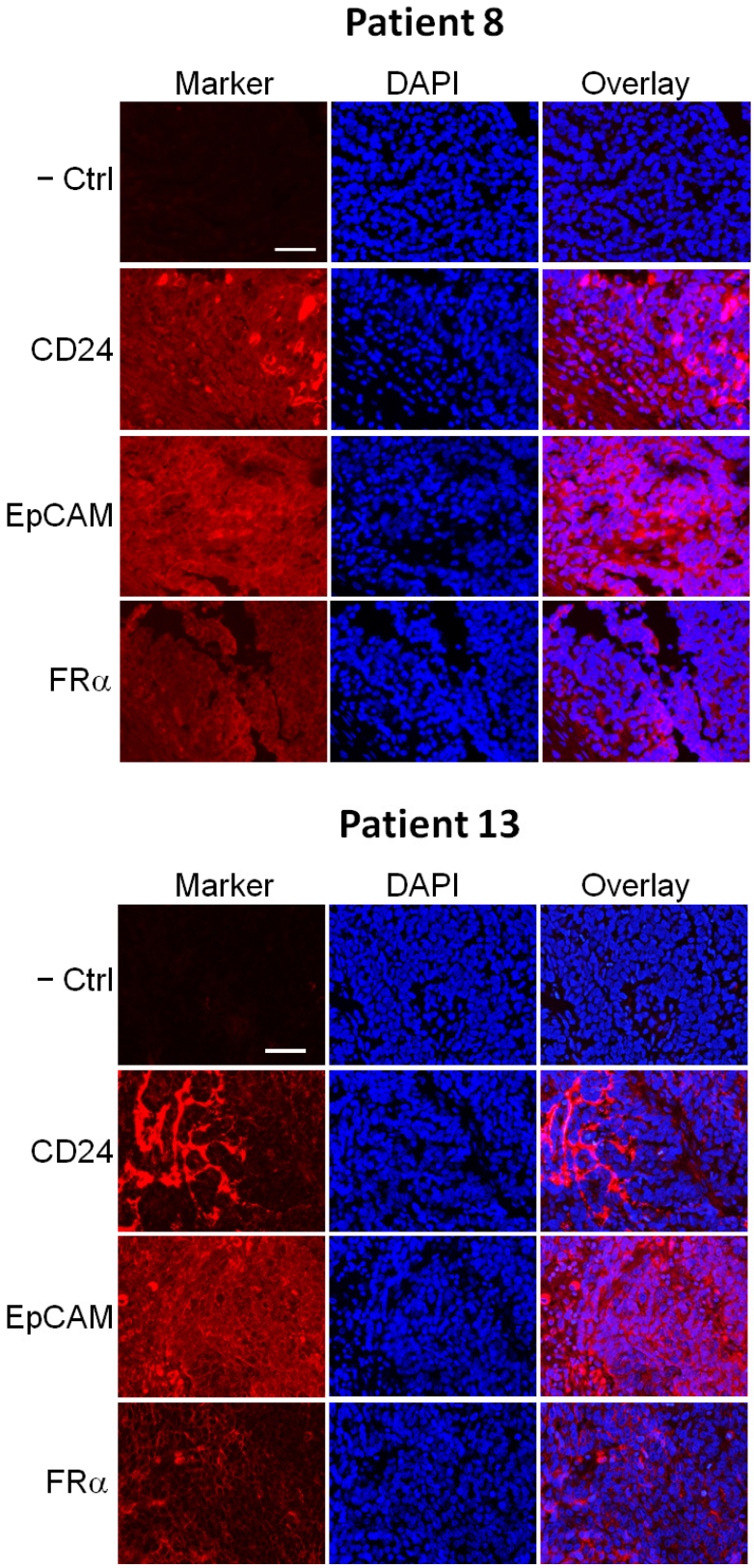

Figure S22. Typical images of immunofluorescence histological assays of the tumor tissues from patients #8 and #13. Scale bar, 50 μm.

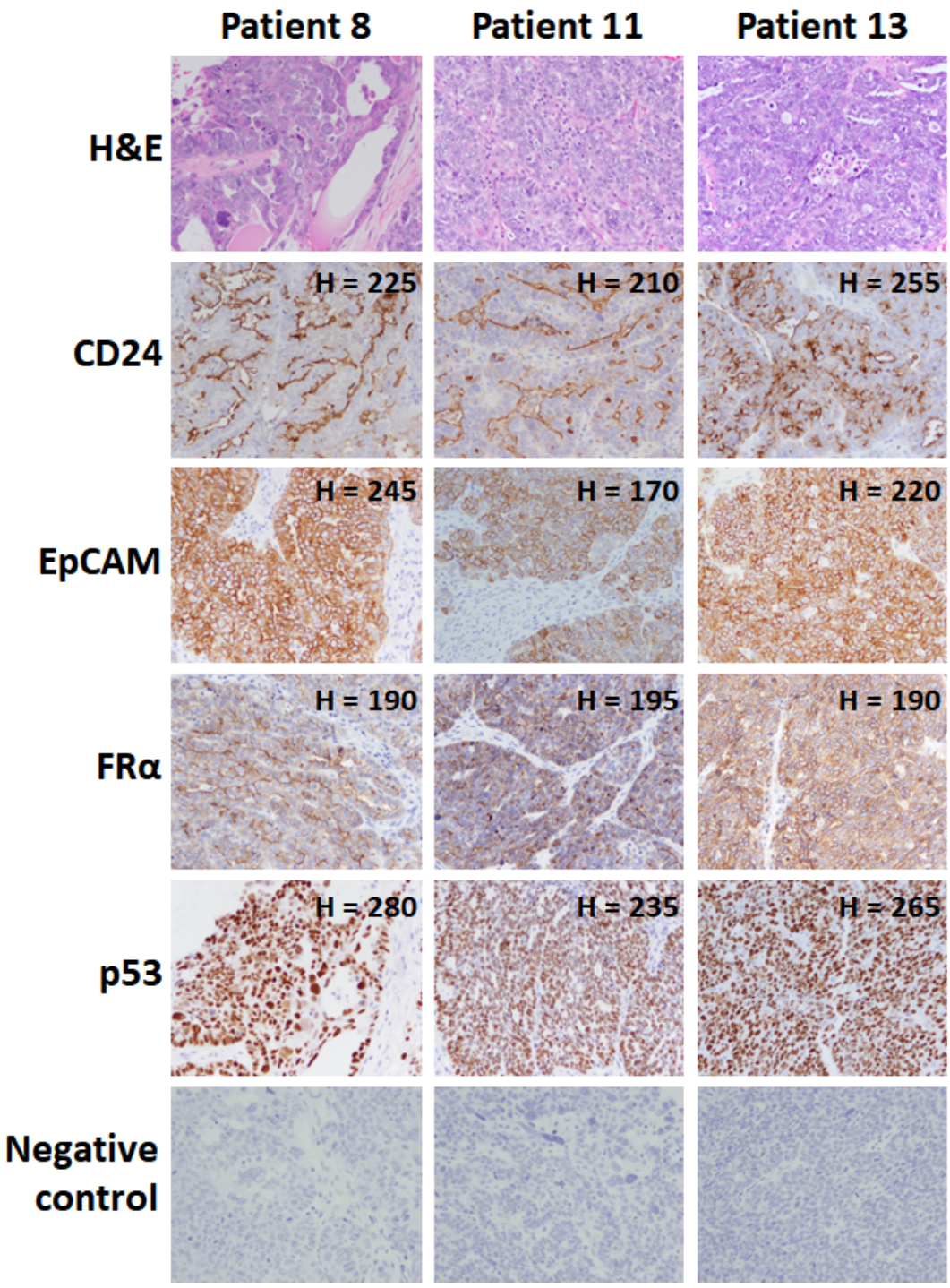

Figure S23. **Representative images of H&E and IHC staining for CD24, EpCAM, FRα, and p53 in patient-matched tumor tissues** (at 20× magnification). p53 is included in the assay as it is typically overexpressed in a majority of serous carcinomas. H scores were derived following pathologist review of the epithelial component of the IHC stained tissue [sum of staining intensity (0, 1+, 2+, or 3+) multiplied by percentage of positive stained cells]. The subcellular localization was apical/luminal membranous and cytoplasmic staining for CD24, membranous and cytoplasmic staining for FRα, membranous staining for EpCAM, and nuclear staining for p53.

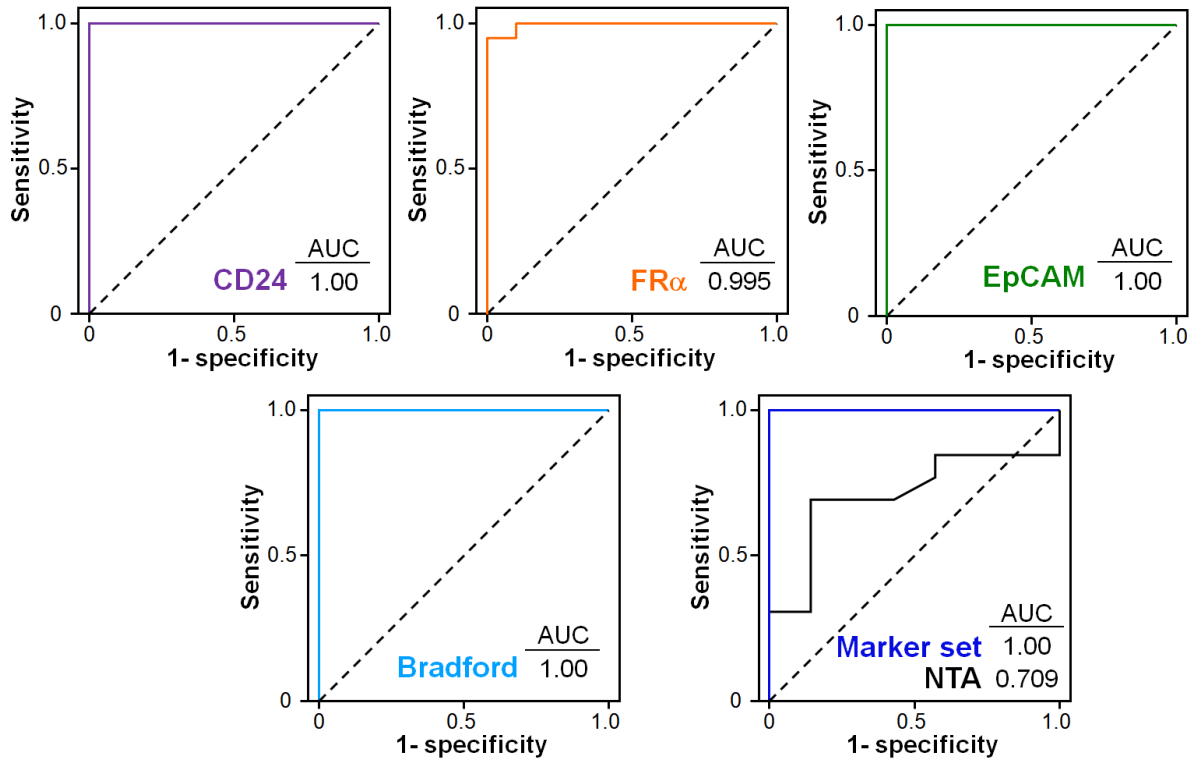

Figure S24. ROC evaluation of diagnostic accuracy of the exosomal biomarkers and exosome counting for OvCa. The ROC curves were plotted using the protein levels of exosomal CD24, EpCAM and FRα in Figure 5e and the NTA data in Figure S16. For the combined three-marker set, the arithmetic average of their levels was used as an independent variable. The area under the curve (AUC) for CD24, EpCAM, FRα, total protein by Bradford assay, the marker set, and EV counts was determined to be 1.00, 1.00, 0.995, 1.00, 1.00, and 0.709, respectively. 95% confidence interval (CI) was used for the statistical analysis.